Received 31 March 2022; revised 13 May 2022; accepted 23 May 2022. Date of publication 30 May 2022; date of current version 7 June 2022.

*Digital Object Identifier 10.1109/OJAP.2022.3178840*

# Multiobjective Fitness Functions With Nonlinear Switching for Antenna Optimizations

**MD RAYHAN KHAN (Graduate Student Member, IEEE), CONSTANTINOS L. ZEKIOS (Senior Member, IEEE), SHUBHENDU BHARDWAJ (Member, IEEE), AND STAVROS V. GEORGAKOPOULOS (Senior Member, IEEE)**

Department of Electrical and Computer Engineering, Florida International University, Miami, FL 33199, USA

CORRESPONDING AUTHOR: MD RAYHAN KHAN (e-mail: mkhan118@fiu.edu)

This work was supported by the Air Force Office of Scientific Research under Grant FA9550-18-1-0191.

**ABSTRACT** In a multi-objective optimization process, several goals are traditionally combined into a single fitness function. In such cases, the choice of the objective function is critical, as it should accurately represent the desired optimization goals. Here, we introduce a new class of multi-objective functions with non-linearity and switching behavior, and also provide a method for *objective function engineering*. Notably, the proposed objective functions introduce versatile forms of fitness growth during the optimization, and provide a systematic approach for integrating the expertise in antenna design with the optimization process. The proposed optimization processes are applied in antenna optimization to demonstrate their enhanced performance. Our optimization examples consider problems based on both analytical electromagnetic models and full-wave simulation. Specifically, we consider the designs of an end-fire array, a pyramidal horn antenna, a Yagi-Uda array, and a wideband patch antenna. Our results suggest that, with minimum computation effort, the proposed non-linear fitness functions produce better performing designs when compared to a linear summation-based fitness function, e.g., 12% higher forward gain for the Yagi-Uda array, 9.3% lower side lobe level for the horn antenna, 23.38% higher directivity for the end-fire array, and approximately 1.5 times higher bandwidth for the wideband patch antenna.

**INDEX TERMS** Antenna optimization, cost function, multi-objective functions, non-linear function, particle swarm optimization.

## I. INTRODUCTION

THE DESIGN of antennas for RF applications requires optimization of geometrical parameters. At the same time, multiple goals such as gain, bandwidth, and impedance matching must be met. The key challenge in such optimizations is how to formulate the multivariate fitness functions that relate the RF performance metrics with the antenna geometrical parameters. Often, this dependence exhibits multiple local maxima (or minima), widely varying curvatures and saddle points located across the functional search space. Therefore, such designs are typically non-convex optimization problems. Furthermore, the multi-dimensionality (i.e., multivariate nature) of such problems makes the visualization of input-output relations difficult. Hence, the trial-and-error approach, or the multi-dimensional parametric sweeps do not provide good optimization strategies. Also, to achieve a truly optimized design, the number of testing points, where the design should be tested, increases exponentially as the number of geometrical parameters increases.

In numerical method based RF optimizations, the fundamental requirement of fast convergence toward global extrema requires a reduction in the number of full-wave electromagnetic (EM) simulations. Toward this goal, prior research has provided different approaches to achieve this. For example, heuristic optimization algorithms, e.g., evolutionary optimization algorithms [1], [2], physics-inspired algorithms [3], [4], and swarm-intelligence based algorithms [5]–[8] have produced optimal designs due to their global search characteristics, which stem from randomness,

an inherent feature of these algorithms. To elaborate, such randomness allows the search algorithm to escape local minima or maxima and efficiently explore the entire design space. A comparative performance of heuristic optimization algorithms (e.g., speed of convergence) has been studied [9]–[11]. Among other approaches, surrogate-models (or digital-twins) using kriging interpolation [12], support vector regression [13], random forest algorithm [14] etc., have been applied to reduce the computational effort by replacing the actual problem with an equivalent computationally inexpensive problem. Surrogate modeling approaches have been further improved by using several methods including dimensionality reduction [15], nested kriging [16], [17], and constrained sampling [18], [19]. In general, these methods belong to the *system-by-design* paradigm [20], which is a systematic optimization approach that handles a set of interconnected blocks, each one related to different design operations (e.g., synthesis, analysis, configuration, etc.).

In multi-objective optimizations, *Pareto-front based optimization* [21] is a widely used approach in optimization of conflicting objectives. In this approach, an ideal solution is selected from a set of solutions (or a Pareto-front) with levels of trade-offs between the objectives [22], [23]. The selection is made based on the knowledge of objective priorities (i.e., domain expertise) after the Pareto-front is created. Nonetheless, the computational efficiency of this approach should be carefully considered, since the optimization is directed toward a frontier of points [24], [25]. With an increasing number of objectives, the computational workload to find the Pareto-front is expected to increase exponentially.

In this context, combining many objectives into a single objective function can reduce computational effort since domain knowledge can be integrated into its design, resulting in a single solution rather than a Pareto-front solution. In this approach, different methods have been pursued, e.g., weighted sum of objectives [6], [7], [26]–[32], lexicographic, weighted Tchebycheff, and weighted product methods [33]. Other methods utilize non-linear functions [8], [34] and adaptive (e.g., fuzzy) functions [35], [36] while forming the multi-objective function. In fact, the *weighted sum method* and its variations form a class of optimization methods that are widely adopted in solving EM optimization problems. For example, a variation of this method uses Heaviside switching [37], [38] to set hard limits on specific objectives during the optimization. In such cases, the weights of individual objectives, such as gain, $S_{11}$, etc., can be adjusted to give preference to the desired objectives.

In multi-objective antenna optimization, designing the objective function is an important task, as the composite fitness of a candidate solution should accurately represent the desired antenna design. To address this issue, we propose a scheme for integrating individual optimization goals into composite fitness functions by applying non-linear switching functions to help optimization algorithms in antenna synthesis. Specifically, we utilize the *switching* functions [39], which are used in artificial neural networks and are well-known for their *activation behavior* [40], [41], to adaptively adjust the weights of objectives *during* the optimization process. The proposed scheme includes a class of topological functions to cover various possible scenarios of fitness growth as desired by the user. Furthermore, an objective function design is proposed as a pre-optimization step by plotting objective versus fitness function plots using the proposed functions. Overall, the scheme provides an effective method to engineer objective functions before conducting the full-wave EM simulations, and saves time by solving the problem of designing the objective function. The enhanced performance of our method is proven by applying it for particle swarm optimization (PSO) [42], [43] of the considered antenna examples, namely, an end-fire array, a pyramidal horn antenna, a Yagi-Uda antenna, and a wideband patch antenna.

## II. THE PROPOSED MULTI-OBJECTIVE FUNCTION

For comparison, we first consider the widely used approach of combining several objectives using linearly weighted sum fitness functions. Then, we present our proposed method that incorporates non-linear switching in multi-objective fitness functions.

### A. LINEAR WEIGHTED SUMMATION OBJECTIVE FUNCTIONS

In the linear weighted sum method, the multi-objective function, $F$, can be defined in terms of objectives $x_n$ ($N$ is the total number of objectives) using the relation

$$F = \sum_{n=1}^{N} H_n = \sum_{n=1}^{N} w_n(x_n \pm k_n), \tag{1}$$

where $w_n$ is the weight assigned to the objective parameter $x_n$, and $k_n$ is any constant that may be added to the fitness. The objectives can be antenna performance parameters, including $S_{11}$, bandwidth, and gain. Each parameter $w_n$ controls the weight of the $n^{\text{th}}$ objective and this parameter remains constant through the entire optimization process. Therefore, in this case, the fitness vs. objective curve is linear, as indicated in Fig. 1(a). However, a non-linear gradient could be beneficial, as it would allow the gradient of the fitness vs. objective curve to change as the objective $x_n$ changes during the optimization process, as shown by the curved lines in Fig. 1(a). For example, the weight of an objective can be reduced, or its fitness can be *saturated*, when the objective has reached a desired value. Therefore, non-linearity will eliminate over optimization of objectives.

### B. MOTIVATIONS FOR NON-LINEAR FITNESS FUNCTIONS

Here, we illustrate the advantages of using non-linear switching functions through the following example. Specifically, in (2), (3), and (4), we formulate objective functions using linear weighted sum method and gradually apply

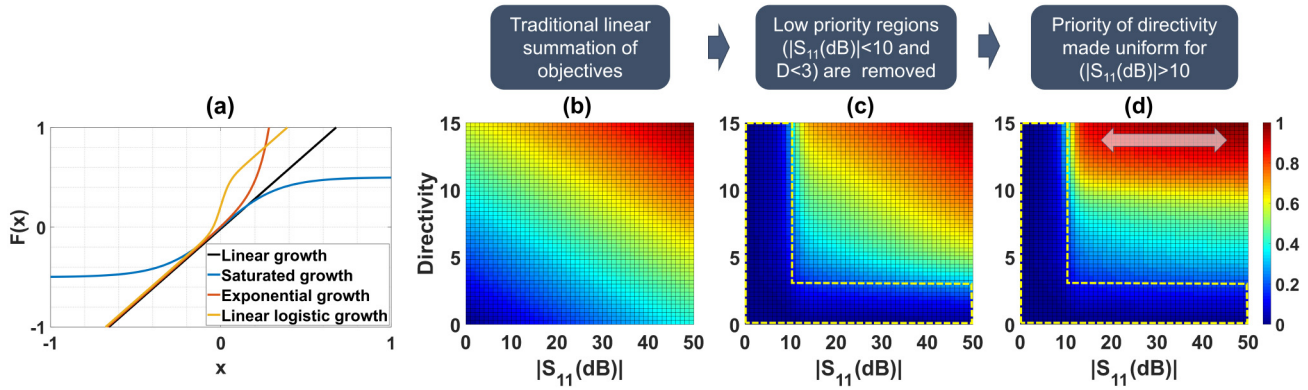


**FIGURE 1.** (a) Comparison of different *y*-normalized fitness growths with respect to an *x*-normalized objective (e.g., $S_{11}$, gain, bandwidth etc.). (b)-(d) Heat map representation for a two-objective (i.e., $|S_{11}|$ and directivity) fitness function using: (b) a linear relation shown in (2), (c) a linear method with activation and saturation terms as in (3), and (d) our proposed method that includes both activation terms and gradient control terms as in (4). The color bar indicates normalized objective function fitness.

non-linear switching on the objective terms. Figs. 1(b)–1(d) illustrate the corresponding objective-space plots of these functions.

$$F = 1 \cdot |S_{11}(dB)| + 5 \cdot D \tag{2}$$

$$F = \text{logsig}(D-3) \times |S_{11}(dB)| + \text{logsig}(|S_{11}(dB)| - 10) \times 5 \cdot D \tag{3}$$

$$F = \text{logsig}(D-3) \times 30 \cdot \tanh\left(\frac{|S_{11}(dB)|}{30}\right) + \text{logsig}(|S_{11}(dB)| - 10) \times (5 \cdot D + 40 \cdot \text{logsig}(D-10)) \tag{4}$$

For this example, $S_{11}$ and directivity, $D$ are chosen as two objectives, and in Figs. 1(b)–1(d), color represents the normalized fitness value. The testing points are scattered in this 2-D search space, and they move to reach the global maximum. Notably, in Fig. 1(b), due to the linear summation, we see a linear gradient with no regard to the RF relevance of the values of $S_{11}$ and $D$. In contrast, by using the non-linear switching functions of (3) and (4), we can control how to explore the 2-D objective space. Specifically, we can achieve the following: (a) reduce the priority of less important regions (i.e., *false-positives*) in the objective space, e.g., $|S_{11}(\text{dB})| < 10$ and $D < 3$, as shown in Fig. 1(c), and (b) provide equal priority to all $|S_{11}(\text{dB})| > 10$ points as long as they exhibit high directivity, as shown in Fig. 1(d).

A second issue of linear summation functions is the over-optimization of a single objective (i.e., *over-fitting*), which can potentially produce designs with high fitness values that are not truly optimal for all objectives. For example, for a typical transceiver application, an antenna with $S_{11}(\text{dB})$ in the order of $-30$ dB offers nearly the same performance as one with $S_{11}(\text{dB})$ in the order of $-40$ dB. However, a design with $S_{11}(\text{dB})$ in the vicinity of $-40$ dB could provide a high fitness value, which can trigger the optimization process to stop, without truly optimizing the values of the other objectives.

### C. FORMULATION OF NON-LINEAR FITNESS FUNCTIONS

The previous section explained the issues of multi-objective optimizations that are based on linear fitness functions and showed the advantages of non-linear fitness functions. In this section, we provide the general mathematical formulation of non-linear multi-objective fitness functions that eliminate the issues of false positives and over-fitting, which significantly slow down the heuristic optimizations. Specifically, we introduce *logistic activation functions*, such as *logsig* and *tanh*, to control the growth rate of each objective, and build a composite fitness function as shown later in (5). The choice of logistic functions is based on their ability to precisely control the objectives' individual growth curves with desired guidelines for gradient, upper limits, and lower limits [44]. Moreover, logistic functions produce objective functions that are continuously differentiable, which is an essential feature in gradient-based optimization algorithms [45]. Even though specific use of *logsig* and *tanh* is shown in this paper, other logistic functions with similar shapes can also be chosen.

The form of our proposed composite fitness function is as following:

$$F = \sum_{n=1}^{N} \left\{ \prod_{m \neq n}^{N} logsig(x_m - b_m) \right\} H_n(x_n) \tag{5}$$

where, $H_n$ is a function of the $n^{\text{th}}$ objective that enables gradient control (i.e., weight adjustment between the objective terms), and can be defined using one of the following forms:

$$H_n(x_n) = sgn(x_n - a_n) \tag{6}$$

$$H_n(x_n) = w_n \cdot (x_n \pm k_n) \pm c \cdot e^{d \cdot (x_n - a_n)} \tag{7}$$

$$H_n(x_n) = w_n \cdot (x_n \pm k_n) \pm sgn(x_n - a_n). \tag{8}$$

In these expressions, $sgn(x)$ denotes the generalized logistic function [44] shown in Fig. 2(d), and can be expressed as:

$$sgn(x) = \frac{U - L}{1 + e^{-\gamma x}} + L \tag{9}$$

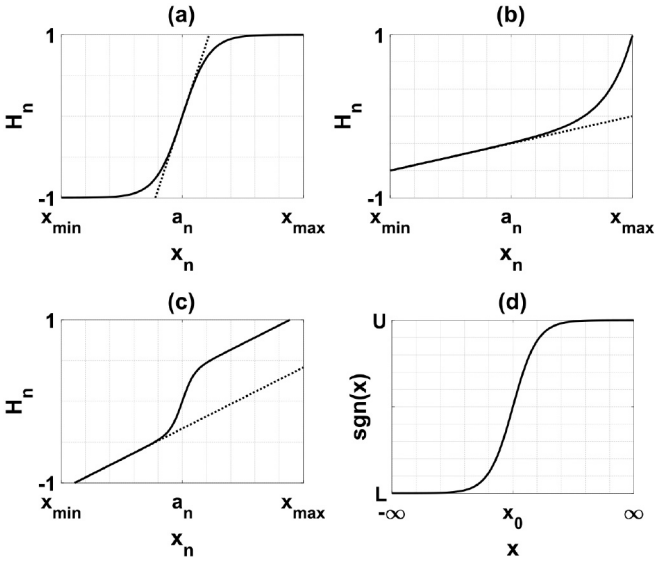


**FIGURE 2.** (a)-(c) Fitness growth curves ($y$-normalized) for the topical functions in (6)-(8). Specifically, (a) shows growth curve for saturated fitness, as per (6), (b) shows growth curve for vigorously increasing fitness, as per (7), and (c) shows growth curve for linearly increasing logistic fitness with desired gradient at threshold, as per (8). (d) A standard logistic function, as per (9).

where $U$ is the upper asymptote, $L$ is the lower asymptote, and $\gamma$ is the rate of initial growth or final decay. The solid lines in Figs. 2(a)–2(c) represent the functions in (6), (7), and (8), respectively. At any point, the weights allocated between the $N$ objectives can be found from the gradients of $H_n$ functions of the respective objectives. Furthermore, the product term, $\prod_{m\neq n}^{N} logsig(x_m - b_m)$ ensures that while improving the fitness of $n^{th}$ objective $x_n$, all other objectives denoted by subscript $m$ are also satisfied beyond the targeted threshold of $b_m$ (i.e., are 'activated'), where $b_m < a_n$. In the following section, we discuss the selection criteria of the individual fitness function, $H_n$ to formulate different types of fitness growth curves that may be desired in an optimization process.

### D. TOPICAL FUNCTION SELECTION

A critical step in multi-objective optimization is the design of objective function, which should be performed according to specific design goals of the problem under study. The design of the proposed composite fitness function introduced in Section II-C is controlled by the selection of the functions in (6)-(8), each representing a unique design scenario. Here, to investigate the performance of the proposed function as in (5), a rigorous analysis is performed with respect to (6)-(8).

First, the function in (6) is used when the optimization goal of an objective has an upper (or lower) limit. In this case, it is desired that the goal does not contribute to the fitness after the objective reaches a certain value. For example, the contribution of an antenna's $S_{11}$ objective to the fitness function should diminish as $S_{11}$ approaches $-30$ dB, since obtaining an $S_{11}$ that is less than $-30$ dB is not typically needed in antennas. In such cases, the choice of (6) allows a gradient decay, as shown in Fig. 2(a), and the fitness of the objective saturates (or reaches a *plateau*). For this case, the upper and lower limits are defined by $U$ and $L$, respectively. Moreover, $\gamma$ controls the gradient around the threshold, and $a_n$ controls the point after which the fitness needs to be saturated. Specifically, higher $\gamma$ corresponds to higher gradient around $a_n$, and vice versa. For instance, if $|S_{11}(\text{dB})|$ is the objective $x_n$, $a_n = 10$ can be considered to begin the gradient decay when $S_{11}(\text{dB}) < -10$ dB. Then, the choice of $U$, $L$, and $\gamma$ can be considered, depending on the desired softness around the plateau. Notably, the initial gradient, i.e., gradient at $x_n = a_n$ of this function is $\gamma(U - L)/4$.

Secondly, for objectives that do not require an upper (or lower) limit (e.g., gain of an antenna), functions in (7) or (8) are respectively chosen, based on the required level of aggression in optimization. For example, (7) provides exponential change in the weight of an objective, with increasing value of the objective, as shown in Fig. 2(b), and this rate is controlled by parameters $c$ and $d$, and threshold point $a_n$. Specifically, higher $d$ with lower $c$ corresponds to steep gradient change around $a_n$, and vice versa. This function is useful when an objective needs to be vigorously optimized near a known or estimated objective extremum, e.g., axial ratio of a circularly polarized antenna. Finally, the function in (8) changes the gradient of an objective within limits, and around a threshold point, $a_n$, using linearly increasing logistic function, as shown in Fig. 2(c). Here, $\gamma$ controls the rate of gradient rise or decay around the threshold point, $a_n$, and $U$ and $L$ control the upper and lower limits of the updated gradient. This function is useful when an objective extremum is unknown, thereby, its weight should be updated within a range. For both functions in (7) and (8), the general linear term, $w_n \cdot (x_n \pm k_n)$, with fixed gradient, $w_n$, defines the linear fitness in the pre-threshold regime, i.e., $x_n < a_n$.

To select one of (6), (7), and (8), along with a suitable set of different parameters, and to ultimately formulate a fitness function that appropriately represents the optimization goals, the following steps are suggested:

- Set the fixed weights, $w_n$, based on the priority of the objectives.
- Select a non-linear function from (6), (7), and (8) for each objective, based on the use cases elaborated in the preceding paragraphs of this section.
- Plot the individual fitness functions, as shown in Figs. 2(a)–2(c) with arbitrary values of the hyper-parameters, e.g., $c$, $d$, $\gamma$, $a_n$ etc.
- Tune the hyper-parameters by observing the individual fitness function plots mentioned in the previous step.
- Apply the desired activation terms [e.g., the $logsig(x_m - b_m)$ terms in (5)] on the individual fitness function and form the composite fitness function, $F$.
- Further tune the hyper-parameters, if needed, with the help of 2-D objective-space plots (or heat maps), as

shown in Figs. 1(b)–1(d). For $N$ objectives, $\binom{N}{2}$ number of 2-D heat maps will be required.

We note that the preceding steps to appropriately formulate a fitness function can be conducted without running a full-wave EM analysis, which saves significant time, and is a practical method for formulating the composite fitness function.

## III. MULTI-OBJECTIVE OPTIMIZATION WITH THE PROPOSED FUNCTION AND RESULTS

The effectiveness of the proposed class of multi-objective functions for electromagnetic optimization is validated through four examples including both analytical design problems and full-wave optimization. As our work focuses on the formulation of objective functions used in optimizations the findings can be applied to various optimization algorithms. Here, to illustrate the performance of our objective functions, we have chosen to use the particle swarm optimization (PSO) algorithm [43]. PSO was chosen due to its ease of implementation, and its well-known applications for antennas [43], [46].

The PSO algorithm uses a population of $N_p$ particles, where each particle explores the search space by updating its 'position' over $N_{iter}$ iterations with the help of its 'velocity'. The position and velocity are calculated using expressions (10) and (11), respectively. Here, $v_i(k)$ and $x_i(k)$ are the velocity and the position of particle '$i$' in the $k^{\text{th}}$ iteration, respectively. In addition, $pbest_i(k)$ and $gbest(k)$ are the personal best position of a particle, and the best position among the entire population in the $k^{\text{th}}$ iteration. Also, $c_1$ and $c_2$ are acceleration constants, and $w$ is the inertia term. Finally, *rand1* and *rand2* are uniformly distributed random numbers between 0 and 1. Over the optimization process, PSO requires to evaluate $N_p \times N_{iter}$ candidate solutions. More details of the PSO algorithm are described in [47]. In our optimization examples, the PSO hyper-parameters, namely $c_1$, $c_2$ and $w$, are taken from [48]. To set an upper limit on the number of objective function evaluation (i.e., total computational time), $N_p$ is set to 30, as suggested in [43], and $N_{iter}$ is set to 20, unless it is stated otherwise.

$$v_i(k+1) = w \cdot v_i(k) + c_1 \cdot rand1 \cdot [pbest_i(k) - x_i(k)] + c_2 \cdot rand2 \cdot [gbest(k) - x_i(k)] \quad (10)$$

$$x_i(k+1) = x_i(k) + v_i(k+1) \quad (11)$$

For each antenna design problem, we consider a comparison between the objective functions using linear summation shown in (1), and non-linear summation shown in (5). Moreover, the objective vs. fitness curves were designed to have the same gradient up to, or near the threshold point. This is illustrated in Figs. 2(a)–2(c) for a single objective variation. Also, the linear summation function does not contain activation function terms. As shown in Figs. 2(a)–2(c), at, or near the threshold point (e.g., $x_n = a_n$), all the curves exhibit the same gradient. The hyper-parameters of (1) and (5), e.g., $w_n$, $a_n$, $b_m$, $\gamma$ etc., are arbitrarily chosen before running the optimizations with a view to achieve an optimal set of objectives for the respective design problems. The conditions relating the initial gradients of $H_n$ in (1), and (5) are summarized in Table 1. Finally, to compare the numerical efficiency of the proposed approach with respect to Pareto-front optimization, each optimization problem is solved using the multi-objective PSO (MOPSO) algorithm [49]. Hyper-parameters for the Pareto-front search are also taken from [49]. The considered optimization problems are elaborated in the following subsections.

**TABLE 1.** Fitness gradient of an objective in the two multi-objective functions and parameter constraints.

| Linear | | Proposed | Parameter constraints |
|---|---|---|---|
| $H_n$ | | $\frac{dH_n}{dx_n}$ | |
| | (6) | $\gamma(U-L)\cdot\frac{e^{-\gamma(x_n-a_n)}}{\left[1+e^{-\gamma(x_n-a_n)}\right]^2}$ | $\frac{dH_{n,l}}{dx_n}$[a] $=$ $\frac{dH_{n,p}}{dx_n}$[b] at $x_n = a_n$ if $\gamma = \frac{4w_n}{U-L}$ |
| $w_n$ | (7) | $w_n + cd \cdot e^{d(x_n-a_n)}$ | $\frac{dH_{n,l}}{dx_n} \approx \frac{dH_{n,p}}{dx_n}$ at $x_n < a_n$ for certain $c$ and $d$ |
| | (8) | $w_n + \gamma(U-L)\cdot\frac{e^{-\gamma(x_n-a_n)}}{\left[1+e^{-\gamma(x_n-a_n)}\right]^2}$ | $\frac{dH_{n,l}}{dx_n} \approx \frac{dH_{n,p}}{dx_n}$ at $\lvert x_n\rvert > a_n$ |

[a] Gradient of the linear fitness function.

[b] Gradient of the proposed non-linear fitness function.

### A. OPTIMIZATION OF A LINEAR END-FIRE ARRAY

As our first optimization problem, we consider the design of a uniformly spaced and uniform amplitude 10-element end-fire array, as shown in Fig. 3(a), where the optimization of excitation phases and inter-element spacing is pursued. The goal is to obtain a highly directive end-fire array. The end-fire array design is a well-known problem with analytical solutions. Specifically, an end-fire radiation criterion is achieved by maximizing the array factor function along $\theta = 0°$ using the condition, $\beta = -kd$ [50, p. 299], where $\beta$ is the phase lag between the elements, and $k = 2\pi/\lambda$. The parameter $d$ represents the inter-element spacing and for an end-fire radiation, $d$ should be less than half a wavelength. Also, end-fire array directivity maximization is proposed in the Hansen-Woodyard design, which provides higher directivity than the ordinary end-fire array by using the criteria $d \approx \lambda/4$, and $\beta \approx -kd + 2.92/N$, where $N$ is the number of array elements [50, p. 304].

Notably, further enhancement of directivity is possible, if optimization is pursued for parameters $d$ and $\beta$, since Hansen-Woodyard design uses approximations. Such optimization is performed here by pursuing the following three goals: (1) maximization of the end-fire directivity (i.e., maximization of the array factor in the end-fire direction

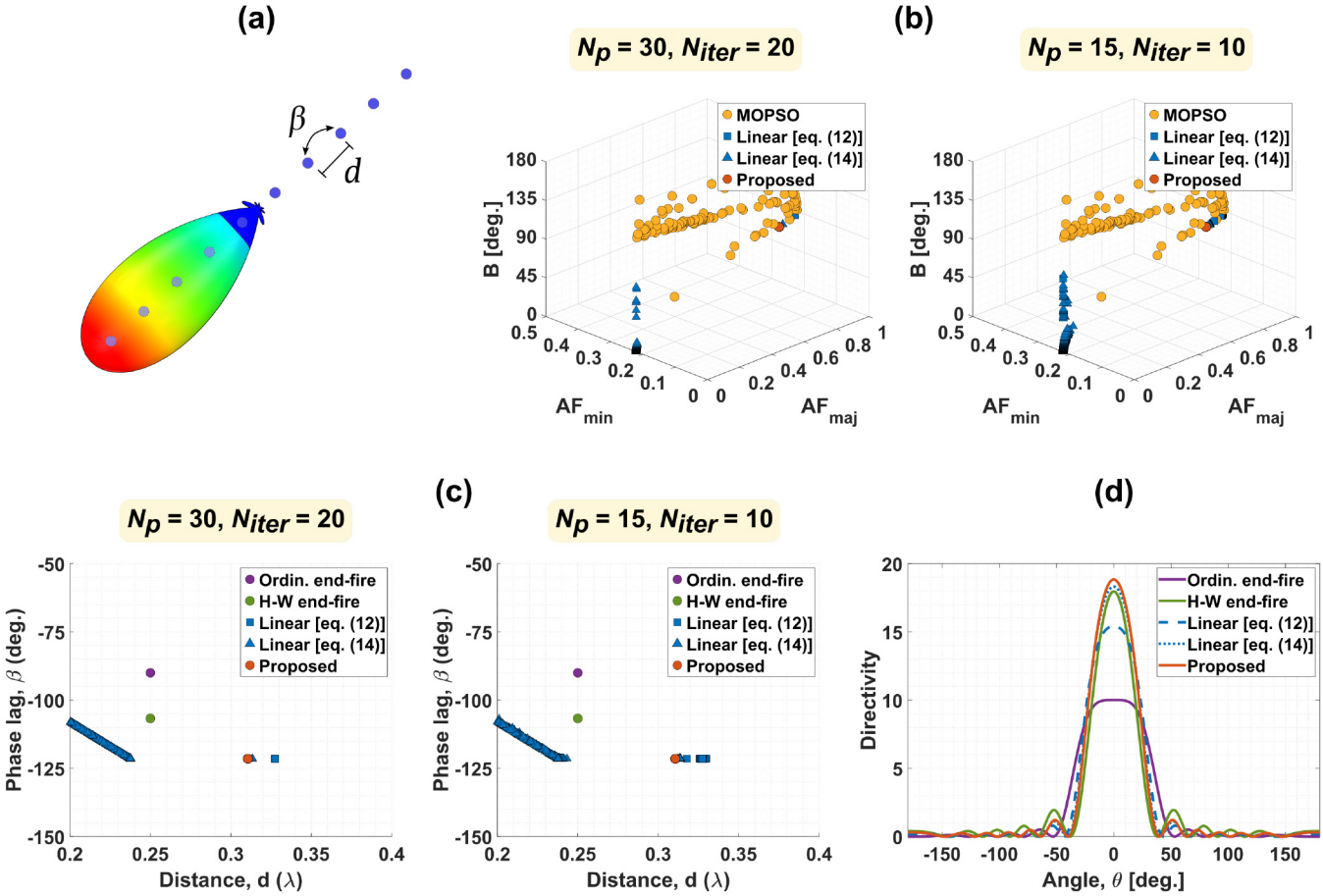


**FIGURE 3.** (a) Geometry of a uniformly spaced and phased end-fire array, (b) objective space for Pareto-front search (denoted by yellow points) using the MOPSO algorithm [49] and for all PSO runs (denoted by blue and orange points). During optimization, results under two algorithm configurations (e.g., $Np = 30$, $N_{iter} = 20$, and $Np = 15$, $N_{iter} = 10$) are shown, (c) optimized $d$ and $\beta$ for all 1,000 runs under the aforementioned PSO configurations compared with a standard end-fire array and a Hansen-Woodyard array, (d) directivity (in linear scale) of the end-fire array for all cases.

of $\theta = 0°$, (2) minimization of the first-null beamwidth (FNBW), and (3) minimization of the first minor lobe or the side lobe level. The design parameters, namely, $d$ and $\beta$ are searched in the range of $d \in \{0.2d_{qw}, 1.5d_{qw}\}$, where $d_{qw} = \lambda/4$ and $\beta \in \{-1.5kd_{qw}, -0.5kd_{qw}\}$. Isotropic radiators were used to represent the array elements. The chosen multi-objective optimization functions for the typical linear summation method, and the proposed non-linear method are shown in (12), and (13), respectively,

$$F = 2 \cdot AF_{maj} + 2 \cdot (-AF_{min} + 1) + 1 \cdot (-B + \pi) \quad (12)$$

$$\begin{aligned} F = {} & A_{AF_{min}} \times A_B \times sgn(-2AF_{maj})_{U=2,L=-2,\gamma=2} \\ & + A_{AF_{maj}} \times A_B \\ & \times \left[2 \cdot (-AF_{min} + 1) + \tanh\left(\frac{-AF_{min} + 0.3}{0.1}\right)\right] \\ & + A_{AF_{maj}} \times A_{AF_{min}} \times \left[(-B + \pi) - e^{\frac{2}{3}\cdot(B-5)}\right] \end{aligned} \quad (13)$$

where, $AF_{maj}$, $AF_{min}$, and $B$ represent the value of the array factor at $\theta = 0°$ [50, p. 295], the value of the array factor at the first minor lobe, and the first-null beamwidth (in radians), respectively, whereas $A_{AF_{maj}}$, $A_{AF_{min}}$, and $A_B$ are the three activation terms of (13) involving $AF_{maj}$, $AF_{min}$, and $B$ respectively, and are defined as $A_{AF_{maj}} = logsig(-AF_{maj} + 0.3)$, $A_{AF_{min}} = logsig(-AF_{min} + 0.6)$, and $A_B = logsig(B - \frac{83}{99}\pi)$. Notably, the two functions were designed so that they follow the constraints mentioned in the last paragraph of Section III, and in Table 1. Gradient control component, $H_n$, for this optimization problem is shown in Table 2. Afterward, the objective coefficients of the linear function of (12) are updated as shown in (14) in an attempt to apply gradient changes similar to (13), and the optimizations are repeated with the updated linear function.

$$F = 1 \cdot AF_{maj} + 2 \cdot (-AF_{min} + 1) + 1 \cdot (-B + \pi) \quad (14)$$

As this study uses analytical calculations for each testing point, it allows us to consider more ensemble attempts. Specifically, the PSO optimizations were repeated 1,000 times for observing the variations resulting from the heuristic nature of the optimization algorithm. The optimized objectives obtained using the objective function-based optimization and the Pareto-analysis are shown in Fig. 3(b). Also, the optimized values of $\beta$ and $d$, as an outcome of these attempts with reference to the designs of the ordinary end-fire

**TABLE 2.** Gradient control component, $H_N$, for the end-fire array optimization using our proposed objective function.

| Objective | Selected equation | Desired gradient control |
|---|---|---|
| Array factor at $\theta = 0°$, $AF_{maj}$ | (6) | Decrease and reach plateau |
| Array factor at first minor lobe, $AF_{min}$ | (8) | Increase within a range |
| First-null beamwidth, $B$ | (7) | Increase indefinitely |

**TABLE 3.** Summary of optimization results for the end-fire array.

| | | Ordinary end-fire array | End-fire array with Hansen-Woodyard conditions | End-fire array optimized with linear objective function | End-fire array optimized with adjusted linear objective function | End-fire array optimized with proposed objective function |
|---|---|---|---|---|---|---|
| Parameters | $d$ | $0.25\lambda$ | $0.25\lambda$ | $0.3275\lambda$ | $0.3134\lambda$ | $0.3106\lambda$ |
| | $\beta$ | $-90°$ | $-106.7°$ | $-121.5°$ | $-121.5°$ | $-121.5°$ |
| Results | $D^{(a)}$ | 10.206 | 18.036 | 15.7 | 18.37 | 19.37 |
| | $B_H{}^{(b)}$ | 69.2° | 38.2° | 52.9° | 41.1° | 38.5° |

(a) Directivity at $\theta = 0°$ (in linear scale).

(b) Half-power beamwidth (in degrees).

array ($d = \lambda/4$, $\beta = -kd$) and the Hansen-Woodyard array ($d = \lambda/4$, $\beta = -kd + 2.92/N$), are shown in Fig. 3(c). The optimizations were repeated with a smaller population size ($N_p = 15$) and a fewer number of iterations ($N_{iter} = 10$) to observe the change in optimization results for both type of functions. Under both PSO configurations (e.g., $N_p = 30$, $N_{iter} = 20$ and $N_p = 15$, $N_{iter} = 10$), we observe that, the linear objective function lead to a broader range of solutions when compared to the proposed function. This indicates that, under limited computational resources, the proposed function is more likely to find 'good' solutions, due to the reduction of 'false-positive' regions and gradient control, when compared to the linear objective functions.

Fig. 3(d) compares the directivity of our optimized designs (based on our proposed and the linear objective functions with $N_p = 30$ and $N_{iter} = 20$) with the directivity of the ordinary and Hansen-Woodyard end-fire arrays. Notably, the best designs from each objective function is chosen. Also, Table 3 summarizes the details and performance of all these designs. There is a difference of approximately 15° in phase and $0.07\lambda$ in inter-element spacing between the optimized design by our proposed method and the Hansen-Woodyard array. Also, the optimized array by our proposed function provided at least 23.38% higher directivity, and 27.2% narrower beam than the one with the initial linear objective function in (12). Notably, the Hansen-Woodyard condition was derived to maximize the directivity for infinitely large end-fire arrays. Since our analysis was performed for a 10-element array, this condition might not provide maximum directivity. Our heuristic optimization based on the proposed non-linear objective function allows slightly better optimization. Specifically, we achieved 7% higher directivity with our proposed objective function than the Hansen-Woodyard end-fire array. On the other hand, the linear objective function resulted in improved directivity pattern after adjusting the objective weights, as shown in (14). Notably, we may have to make multiple optimization attempts by adjusting the linear objective function's weights, or providing additional iterations for the optimization process, to converge to an optimal solution, which increases the computational cost significantly.

In this example, all the experiments were completed under a minute, since the analytical expressions for calculating the end-fire array directivity are computationally inexpensive. However, with both type of objective functions (e.g., linear and proposed), the number of design evaluations were significantly lower than the Pareto-front search. Specifically, during the Pareto-front search, 10,000 designs were evaluated (with $N_p = 100$, and $N_{iter} = 100$) whereas the objective functions needed only 600 design evaluations in each optimization attempt, which reduced the computational time by a factor of approximately 16.67. However, within these 600 design evaluations, the optimization result of the proposed objective function was significantly better (e.g., 23.38% higher directivity) when compared to the result of the traditional linear objective function.

### B. OPTIMIZATION OF A PYRAMIDAL HORN ANTENNA

As our second optimization problem, we consider the radiation pattern optimization of an X-band pyramidal horn antenna, as shown in Fig. 4(a), at 10 GHz frequency. High directivity and low side lobe level are typically desired from such antenna. The far-field radiation characteristics of a horn antenna can be controlled by changing the E-plane and H-plane flare angles ($\psi_e$ and $\psi_h$, respectively), and the effective length of the horn ($\rho$), which is the distance of the horn aperture from the phase center. Optimization of horn antennas is commonly pursued using heuristic methods [51], [52] due to its multi-dimensional nature.

In practice, the effective length and the flare angles can be controlled by changing the horn length, $P$, and the aperture dimensions, $a_1$ and $b_1$, respectively. At 10 GHz, a standard 20 dB horn antenna design is given in [50, p. 749]. Here, we pursue directivity enhancement and side lobe level reduction of this reference antenna by considering $P$, $a_1$, and $b_1$ as variables. We define three goals, namely, (1) maximization of directivity along the horn axis (i.e., along $z$ axis), (2) minimization of the side lobe level at the E-plane, and (3) minimization of the half-power beamwidth, to enhance the antenna directivity. It is worth noting that, the third objective is pursued with a view to supplement the

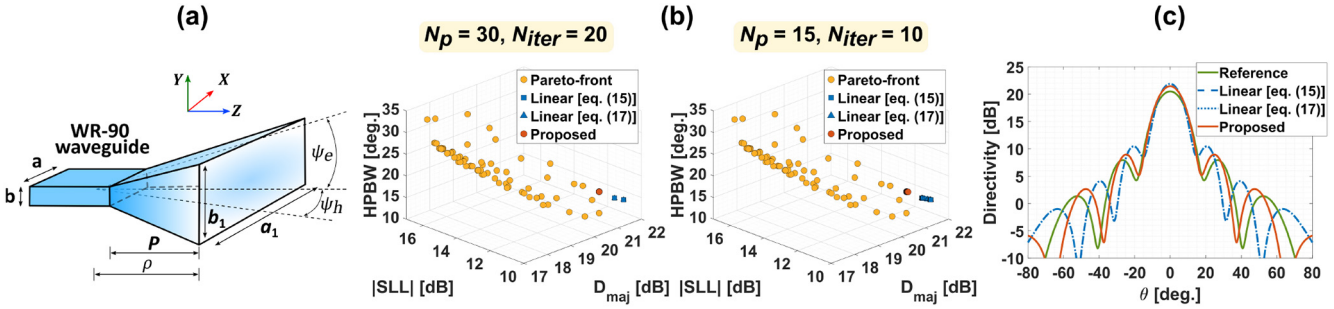


**FIGURE 4.** (a) Geometry of a pyramidal horn antenna, (b) objective space for Pareto-front search (denoted by yellow points) using the MOPSO algorithm [49] and for all PSO runs (denoted by blue and orange points). Optimization results under two PSO algorithm configurations (e.g., $N_p = 30$, $N_{iter} = 20$, and $N_p = 15$, $N_{iter} = 10$) are shown, (d) E-plane directivity (in dB scale) of the horn antenna for all cases.

improvement of the first goal (e.g., directivity). Moreover, the search space for the three parameters are $P \in \{8\lambda, 10\lambda\}$, $a_1 \in \{3\lambda, 5\lambda\}$, and $b_1 \in \{2\lambda, 4\lambda\}$, where $\lambda$ is the wavelength at 10 GHz frequency. The analytical expression in [50, p. 750] is used to calculate far-field directivity along the E-plane (e.g., $y$-$z$ plane). We compare the optimization results involving the linear objective function in (15) and the proposed objective function in (16),

$$F = 2 \cdot D_{maj} + 1 \cdot |SLL| + 1 \cdot (-B_{hp} + 60) \tag{15}$$

$$\begin{aligned} F = {} & A_{SLL} \times A_{B_{hp}} \\ & \times \left[2 \cdot D_{maj} + sgn(D_{maj} - 19)_{U=20,L=0,\gamma=1}\right] \\ & + A_{D_{maj}} \times A_{B_{hp}} \\ & \times \left[1 \cdot |SLL| + sgn(|SLL| - 12)_{U=20,L=0,\gamma=0.4}\right] \\ & + A_{D_{maj}} \times A_{SLL} \\ & \times \left[-B_{hp} + 60 - sgn(B_{hp} - 25)_{U=20,L=0,\gamma=0.4}\right] \end{aligned} \tag{16}$$

where $D_{maj}$, $SLL$, and $B_{hp}$ are the directivity (in dB) along the horn axis, the side lobe level (in dB), and the half-power beamwidth, respectively. Moreover, $A_{D_{maj}}$, $A_{SLL}$, and $A_{B_{hp}}$ are the three activation terms of (16) involving $D_{maj}$, $SLL$, and $B_{hp}$, and are defined as $A_{D_{maj}} = logsig(D_{maj} - 17)$, $A_{SLL} = logsig(|SLL| - 8)$, and $A_{B_{hp}} = logsig(-B_{hp} + 30)$, respectively. Similar to the example in Section III-A, the two functions are designed following the constraints mentioned in Table 1. Finally, we update the gradients of (15), as shown in (17), to achieve results similar to the ones we expect to obtain with (16).

$$F = 5 \cdot D_{maj} + 2 \cdot |SLL| - 1 \cdot (B_{hp} - 60) \tag{17}$$

Fig. 4(b) shows the optimized objectives for different types of objective functions under two PSO configurations placed next to the MOPSO results. Here, the linear objective function converged to multiple distant points, similar to the results obtained in Section III-A, Fig. 3(b). Also, when fewer PSO particles and iterations are utilized, the use of the linear objective function results to solutions, scattered in a wide range of 'optimal' solutions, compared to the solutions of the proposed objective functions that are more clustered [see Fig. 4(b). Therefore, results with the proposed function shows high robustness with the reduction of computational resources.

Fig. 4(c) shows the far-field directivity (E-plane) for optimized horn antennas obtained from optimizations using different objective functions. Here, patterns for the median designs are shown, e.g., $(P_e, a_1, b_1) = (10\lambda, 5\lambda, 3.8325\lambda)$ for the linear function in (15), $(P_e, a_1, b_1) = (10\lambda, 5\lambda, 3.8327\lambda)$ for the linear function in (17), and $(P_e, a_1, b_1) = (10\lambda, 5\lambda, 3.2975\lambda)$ for the proposed function in (16). Both the linear and the proposed objective functions have nearly same directivity along $\theta = 0°$ (linear function results in only 1% higher directivity). However, the side lobe level from the proposed objective function is 9.3% lower than the ones from the linear functions. Although the half-power beamwidth with the proposed function is larger by 2°, the desired goals of directivity maximization and side lobe level reduction is achieved with the proposed objective function. Notably, adjusting the linear objective function did not provide significant side lobe level reduction, indicating the necessity for additional weight adjustments and optimization repetition.

In this example, the objective function-based optimization (with $N_p = 30$, and $N_{iter} = 20$) needed approximately 10 minutes to converge to an optimal solution, whereas, the Pareto-front discovery effort (with $N_p = 100$, and $N_{iter} = 100$) required approximately 2 hours and 47 minutes. This suggests a minimum computational cost reduction by a factor of 16.67 with the objective function approach when compared to the Pareto-front search using MOPSO algorithm. Nonetheless, with a fixed number of objective function evaluation, better performing designs (e.g., 9.3% lower side lobe level) can be achieved using the proposed function when compared to the traditional linear objective function.

### C. OPTIMIZATION OF A FIVE-ELEMENT YAGI-UDA ANTENNA ON A MIURA-ORI SUBSTRATE

As our third example, we consider a full-wave numerical analysis based optimization of a five-element Yagi-Uda antenna designed on a Miura-Ori substrate, as shown in Fig. 5(a). Recently, Miura-Ori [53] patterns have been proposed for reconfigurable and deployable antennas.

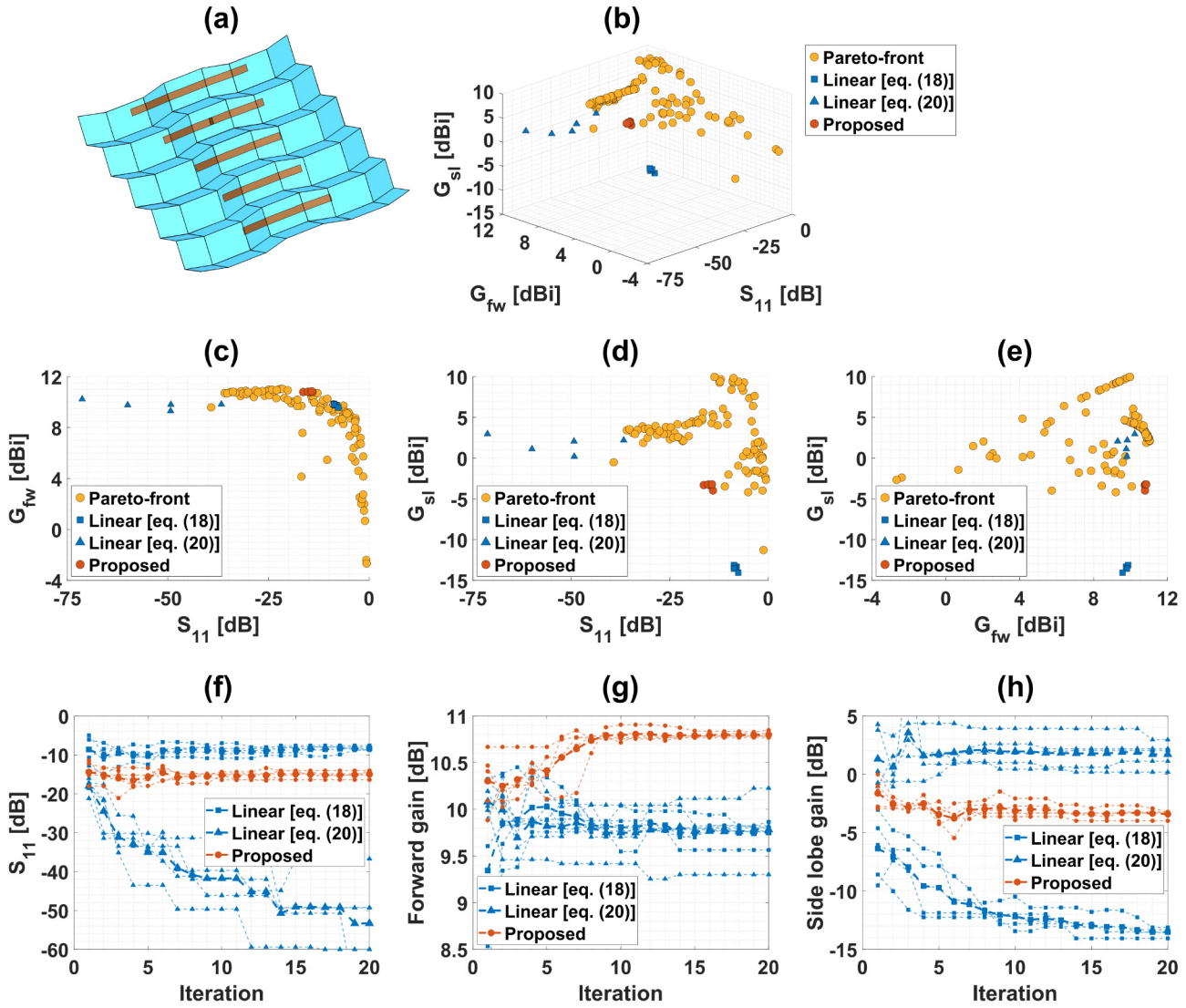


**FIGURE 5.** (a) Yagi-Uda antenna on Miura-Ori substrate, (b) objective space for the optimized designs obtained using different methods, (c)-(e) two- objective plots for the optimized designs obtained using different methods, (f)-(h) evolution of different design objectives over PSO iterations of the Yagi-Uda antenna.

Miura-Ori represents a class of origami with a systematic mathematical formulation for folding and unfolding. But this design comes at the price of time-consuming geometrical CAD model constructions, and optimizations [54]. Automated optimization using heuristic approaches could play a crucial role for the fast modeling of such designs. Here, optimization was conducted for 6 geometrical parameters, namely, the lengths of the five Yagi-Uda antenna elements and their uniform inter-element spacing, $d$. Notably, the inter-element spacing, $d$, is controlled by the folding angle of the Miura-Ori substrate. The parameter space for this optimization is given in [55]. The optimization goals of this optimization are good impedance matching, high forward gain, and low side lobe gain. Our origami modeling toolset [55] was used to perform the automated modeling of the Yagi-Uda antenna in ANSYS HFSS.

The two chosen objective functions, which combine the individual goals, based on the typical linear summation method and the proposed non-linear method, are shown in (18) and (19), respectively,

$$F = 1 \cdot (|S_{11}(dB)| - 10) + 5 \cdot \left(G_{fw} - 4\right) + 3 \cdot (-G_{sl}) \quad (18)$$

$$F = A_{G_{fw}} \times A_{G_{sl}} \times 30 \cdot \tanh\left(\frac{|S_{11}(dB)| - 10}{30}\right) + A_{S_{11}} \times A_{G_{sl}} \times \left[5 \cdot \left(G_{fw} - 4\right) + e^{0.7(G_{fw}-5.5)}\right] + A_{S_{11}} \times A_{G_{fw}} \times sgn(-G_{sl})_{U=50,L=-50,\gamma=0.12} \quad (19)$$

where, $G_{fw}$ and $G_{sl}$ are the forward gain (in dBi), and the first side lobe level gain (in dBi), respectively, and $A_{S_{11}}$, $A_{G_{fw}}$, and $A_{G_{sl}}$ are the three activation terms of (19) involving $S_{11}$(dB), $G_{fw}$, and $G_{sl}$, respectively. Specifically, they are defined as $A_{S_{11}} = logsig(|S_{11}(dB)| - 10)$, $A_{G_{fw}} = logsig(G_{fw} - 3)$, and $A_{G_{sl}} = logsig[-(G_{sl} - 1)]$. Similarly to the two previous examples, the choice of different terms in (18) was based on the equal weight constraints near or around the threshold points. The selection of the gradient control component, $H_n$,

**TABLE 4.** Gradient control component, $H_N$, for the Yagi-Uda antenna optimization using our proposed objective function.

| Objective | Selected equation | Desired gradient control |
|---|---|---|
| Reflection coefficient, $S_{11}$(dB) | (6) | Decrease and reach plateau |
| Forward gain, $G_{fw}(dBi)$ | (7) | Increase indefinitely |
| Side lobe gain, $G_{sl}(dBi)$ | (6) | Decrease and reach plateau |

for the three objectives is given in Table 4. Additionally, a second linear objective function, as in (20), which has a different set of weights, is also considered with the goal of optimizing the three objectives. Each objective function was tested via five optimization attempts to observe the statistical variations.

$$F = 3 \cdot (|S_{11}(dB)| - 10) + 3 \cdot \left(G_{fw} - 4\right) + 3 \cdot (-G_{sl}) \quad (20)$$

Figs. 5(b)–5(e) show the optimized objectives found using different objective functions next to the Pareto-front search results. Also, Figs. 5(f)–5(h) show the evolution of $S_{11}$(dB), forward gain, and first side lobe gain of the best solution in each PSO iteration. All five PSO attempts for each objective function are shown by light colored lines and their average is shown by dark colored line. On average, the proposed objective function resulted in lower $S_{11}$(dB), and approximately 11% higher forward gain compared to the designs produced by the linear objective function in (18). However, the linear function resulted in significantly lower side lobe gain, which indicates over-optimization of the side lobe objective at the cost of under-optimization of others (e.g., $S_{11}$ and broadside gain). On the other hand, the updated linear objective function in (20) shows over-optimization of $S_{11}$(dB) and under-optimization of the two other objectives. The results clearly highlight the problems associated with the definition of appropriate weights in the linear objective function and also the need for the proposed non-linear objective function, especially for optimizations involving numerical analysis.

Figs. 6(a)–6(c) compare the $S_{11}$ versus frequency, realized forward gain versus frequency, and elevation radiation pattern at 2.1 GHz of the optimized designs produced by the two types of objective functions. It is seen that the proposed objective function provided a well-matched Yagi-Uda antenna at approximately 2.1 GHz, with approximately 12% higher forward gain and good side lobe gain (e.g., approximately 14.5 dB lower than the forward gain) compared to the ones obtained using the linear objective functions.

In this example, total time for each optimization attempt (with $N_p = 30$, and $N_{iter} = 20$) was approximately 20 hours for both types of objective functions. On the contrary, the Pareto-front discovery effort (with $N_p = 50$, and $N_{iter} = 50$) required approximately 83 hours, which

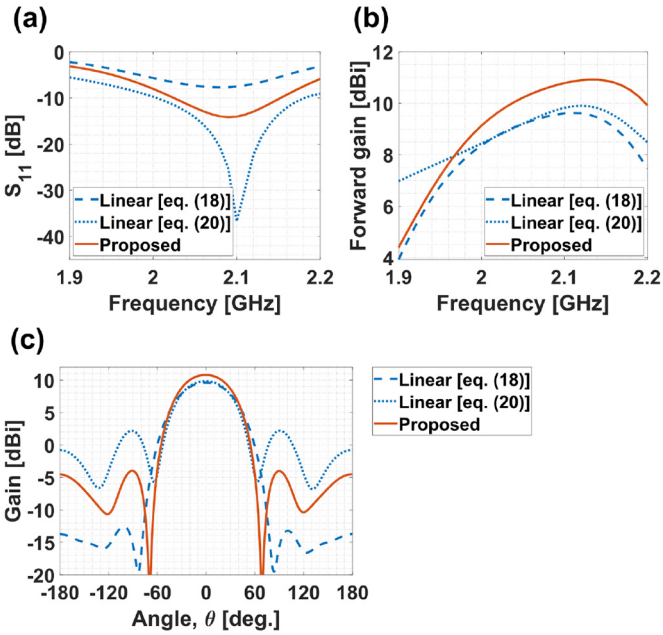


**FIGURE 6.** (a) $S_{11}$(dB) vs. frequency, (b) realized gain (dBi) vs. frequency, and (c) elevation realized gain (dB) at 2.1 GHz for the origami Yagi-Uda antenna.

translates to minimum computational cost reduction by a factor of 4.15 with both types of objective functions (e.g., linear and proposed). In essence, the results suggest that the proposed objective function enables significant computational cost reduction when compared to MOPSO based Pareto-front search, and better performing designs when compared to a linear objective function under identical computational budget.

### *D. OPTIMIZATION OF A PATCH ANTENNA WITH PARASITIC ELEMENT*

As our final example, we consider the optimization of a microstrip patch antenna with U-shaped parasitic elements operating in a band around 5 GHz, as shown in Fig. 7(a). The design is inspired by [56] and is selected due to the widespread relevance of patch antenna designs and large number of parameters in this design. As indicated in Fig. 7(a), the parameters to be optimized are the length, $L$, and width, $W$, of the main patch element, horizontal width, $W'$, and vertical width, $L'$, of the parasitic elements, horizontal gap, $G_W$, vertical gap, $G_L$, gap between two parasitic elements, $G_m$, and the position of the coaxial feed from the edge of the patch element, $d_{feed}$. The range of values considered for the optimization are shown in Table 5. The design used an FR4 substrate with thickness of 4 mm, dielectric constant of 4.4 and a loss tangent of 0.02. The design goals were good impedance matching (low $S_{11}$), high broadside gain, and large impedance bandwidth. The gain was calculated at 5 GHz, and the bandwidth was defined based on the frequencies where $S_{11} \leq -10$ dB. The optimization routine was implemented in MATLAB, and Visual Basic (VB)

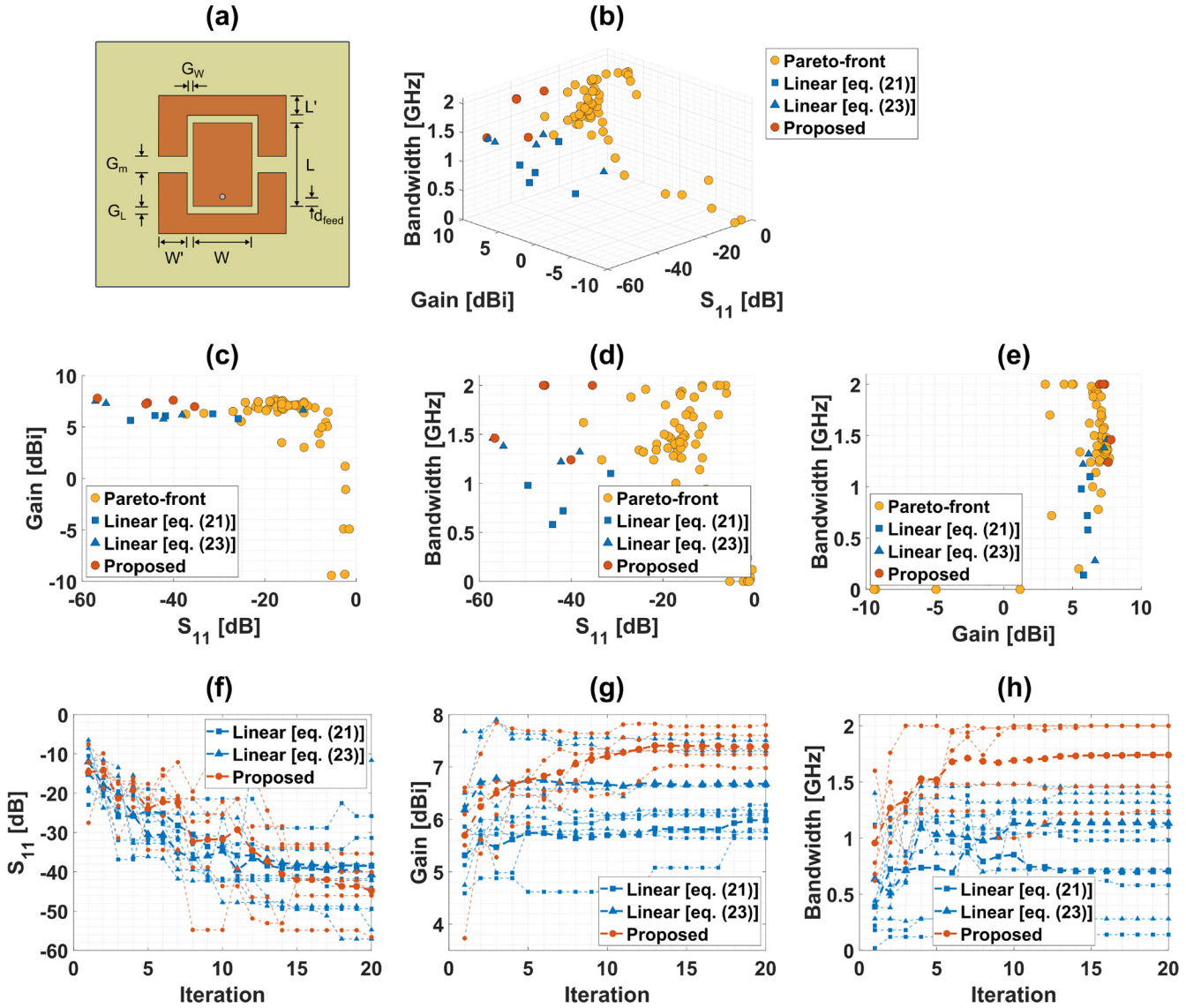


**FIGURE 7.** (a) Microstrip patch antenna with parasitic elements, (b) objective space for the optimized designs using different methods, (c)-(e) two- objective plots for the optimized designs obtained using different methods, (f)-(h) evolution of different design objectives over PSO iterations of the wideband microstrip patch antenna.

scripting was used to interface MATLAB with the ANSYS HFSS full-wave simulation software.

For the optimization of the patch antenna considered here, the performance of the typical linear summation objective function shown in (21), and the proposed non-linear objective function shown in (22) is compared, where $G$ is the broadside gain in dBi, $BW$ is the bandwidth, and $A_{S_{11}}$, $A_G$, and $A_{BW}$ are the three activation terms associated with $S_{11}$(dB), $G$, and $BW$ terms, respectively.

$$F = 2.4 \cdot (|S_{11}(dB)| - 10) + 20 \cdot (G - 5) + 20 \cdot BW \quad (21)$$

$$F = A_G \times A_{BW} \times 60 \cdot \tanh\left(\frac{|S_{11}(dB)| - 10}{25}\right) + A_{S_{11}} \times A_{BW} \times \left[20 \cdot (G - 5) + e^{0.5 \cdot G}\right] + A_{S_{11}} \times A_G \times \left[20 \cdot BW + 2 \cdot e^{2 \cdot BW}\right] \quad (22)$$

Specifically, they are defined as $A_{S_{11}} = logsig(|S_{11}(dB)| - 10)$, $A_G = logsig(G - 0)$, and $A_{BW} = logsig(BW - 0)$. Both objective functions have the same weight distribution of goal terms up to their defined corresponding thresholds, as in the previous examples. For our proposed objective function, the gradient components, $H_n$, which were used for the three objectives in this optimization, are defined in Table 6. Furthermore, with the goal of optimizing the three objectives, a second linear objective function is considered, as shown in (23), with a new set of weights. Separate PSO optimizations were performed using (21), (23), and (22), and each objective function was tested over five optimization attempts to observe statistical variations. Both objective functions have the same weight

$$F = 1 \cdot (|S_{11}(dB)| - 10) + 30 \cdot (G - 5) + 30 \cdot BW \quad (23)$$

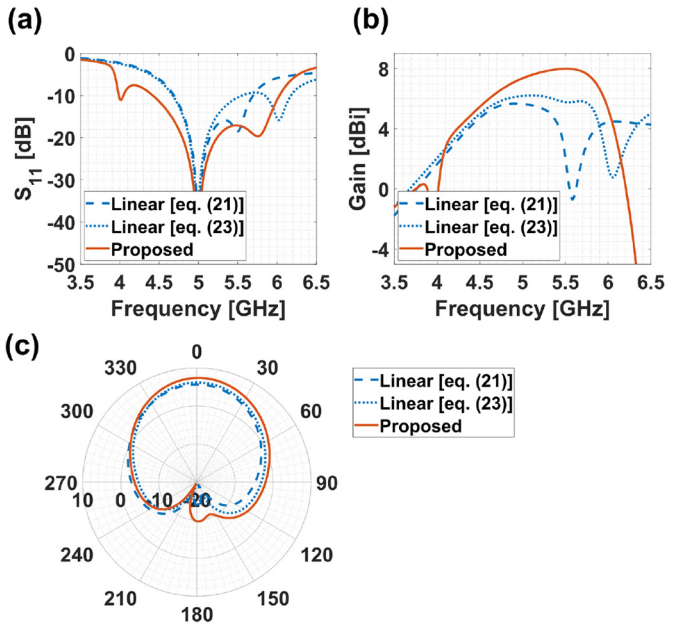


**FIGURE 8.** (a) $S_{11}$(dB) vs. frequency, (b) realized gain (dBi) vs. frequency, and (c) elevation radiation pattern at 5 GHz for the patch antenna.

**TABLE 5.** Specified limits of the optimization parameters for the patch antenna.

| Parameters | Range of the search space |
|---|---|
| $L$ | $0.3\lambda_g$ - $0.6\lambda_g$ [(a)] |
| $W$ | $0.2\lambda_g$ - $0.3\lambda_g$ |
| $W'$ | $0.005\lambda_g$ - $0.5\lambda_g$ |
| $L'$ | $0.005\lambda_g$ - $0.25\lambda_g$ |
| $G_W$ | $0.0025\lambda_g$ - $0.15\lambda_g$ |
| $G_L$ | $0.0025\lambda_g$ - $0.15\lambda_g$ |
| $G_m$ | $0.0025\lambda_g$ - $0.15\lambda_g$ |
| $d_{feed}$ | 0 - $0.3\lambda_g$ |

[(a)] Here, $\lambda_g = 40.45$ mm, which is the guided wavelength, calculated using the formula, $\lambda_g = \frac{c}{f\sqrt{\epsilon_{r,\,eff}}}$ for wavelength, $\lambda = 60$ mm, considering 5 GHz center frequency.

Figs. 7(b)–7(e) show the optimized objectives found using different objective functions next to the Pareto-front search results. Figs. 7(f)–7(h) show the evolution of $S_{11}$(dB), broadside gain, and bandwidth corresponding to the global best solution over the PSO iterations. All five PSO attempts for the objective functions are shown by the light colored lines, and their average value is shown by the dark colored line. On average, when compared to the linear objective functions in (21), and (23), the proposed objective function provided approximately the same return loss. However, 23.6% higher broadside gain, and 147% higher impedance bandwidth was observed on average, when compared to the linear objective function in (21). Also, 10.7% higher broadside gain, and 53.7% higher impedance bandwidth was observed on average, when compared to the updated linear objective function in (23). The performance of three optimized antenna designs,

**TABLE 6.** Gradient control components, $H_N$, for the patch antenna optimization using our proposed objective function.

| Objective | Selected equation | Desired gradient control |
|---|---|---|
| Reflection coefficient, $S_{11}$(dB) | (6) | Decrease and reach plateau |
| Broadside gain, *G(dBi)* | (7) | Increase indefinitely |
| Impedance bandwidth, *BW* | (7) | Increase indefinitely |

produced by the linear and the proposed non-linear objective functions, is compared in Figs. 8(a)–8(c) in terms of $S_{11}$, realized broadside gain (dBi), and radiation pattern at elevation at 5 GHz. In summary, the proposed objective function resulted in a well-matched patch antenna at 5 GHz, with approximately 60% and 32% wider $-10$ dB $S_{11}$(dB) bandwidth, 30% and 19% higher broadside gain at 5 GHz, and more uniform gain performance over a wider frequency band, when compared to the antenna designs calculated by linear objective functions in (21) and (23), respectively. Notably, the non-linear functions applied to the proposed function enabled the PSO algorithm to find better designs with the same number of full-wave simulations. As indicated by our findings, multiple unique sets of objective weights may need to be explored to achieve an appropriate design with the linear objective function.

Each optimization with PSO (with $N_p = 30$, and $N_{iter} = 20$) required approximately 21 hours of time for both types of objective functions. On the contrary, the Pareto-front discovery effort (with $N_p = 50$, and $N_{iter} = 50$) required approximately 88 hours, which translates to minimum computational cost reduction by a factor of 4.2 with both types of objective functions (e.g., linear and proposed). However, as compared to the results of the linear objective function, the optimization result of the proposed objective function was significantly better (e.g., approximately 60% wider bandwidth and 30% higher gain).

## IV. CONCLUSION

In objective function based multi-objective optimizations, the linear weighted sum approach of combining objectives into a composite objective function is limited as it leads to under-fitting and over-fitting. We introduced a new class of objective functions that leverages non-linear properties of switching functions to provide adaptive gradient control, fitness saturation, and threshold features, thereby exploring the search space more optimally. Specifically, our proposed approach eliminates issues of false-positive fitness and over-fitting by integrating domain expertise in the engineered objective function. To validate the performance of our proposed optimization methodology, four antenna optimization problems were considered. The first two optimization problems involved analytical expression-based computation of a 10-element end-fire array and a pyramidal horn antenna. We also optimized an origami Yagi-Uda

antenna, and a wideband patch antenna with parasitic elements to show the effectiveness of our optimization method in full-wave simulations. Our proposed functions produced better designs than the ones provided by linear objective functions for all four problems compared to the linear weighted summation type objective functions. In each case, a cost comparison with a Pareto-front based optimization (e.g., MOPSO) is also presented. In conclusion, our proposed multi-objective functions enable heuristic optimization algorithms, such as PSO, to efficiently find designs in fewer steps, thereby saving computational time and memory.

## REFERENCES

[1] J. S. Smith and M. E. Baginski, "Thin-wire antenna design using a novel branching scheme and genetic algorithm optimization," *IEEE Trans. Antennas Propag.*, vol. 67, no. 5, pp. 2934–2941, May 2019.

[2] R. Jiao, Y. Sun, J. Sun, Y. Jiang, and S. Zeng, "Antenna design using dynamic multi-objective evolutionary algorithm," *IET Microw. Antennas Propagat.*, vol. 12, no. 13, pp. 2065–2072, 2018.

[3] Y. Zhao *et al.*, "Broadband diffusion metasurface based on a single anisotropic element and optimized by the simulated annealing algorithm," *Sci. Rep.*, vol. 6, no. 1, pp. 1–9, 2016.

[4] G. Qubati, R. Formato, and N. Dib, "Antenna benchmark performance and array synthesis using central force optimisation," *IET Microw. Antennas Propag.*, vol. 4, no. 5, pp. 583–592, 2010.

[5] J. Budhu and Y. Rahmat-Samii, "A novel and systematic approach to inhomogeneous dielectric lens design based on curved ray geometrical optics and particle swarm optimization," *IEEE Trans. Antennas Propag.*, vol. 67, no. 6, pp. 3657–3669, Jun. 2019.

[6] C. Zhang, X. Fu, L. P. Ligthart, S. Peng, and M. Xie, "Synthesis of broadside linear aperiodic arrays with sidelobe suppression and null steering using whale optimization algorithm," *IEEE Antennas Wireless Propag. Lett.*, vol. 17, no. 2, pp. 347–350, Feb. 2018.

[7] A. Darvish and A. Ebrahimzadeh, "Improved fruit-fly optimization algorithm and its applications in antenna arrays synthesis," *IEEE Trans. Antennas Propag.*, vol. 66, no. 4, pp. 1756–1766, Apr. 2018.

[8] M. A. Zaman, M. Gaffar, M. M. Alam, S. A. Mamun, and M. A. Matin, "Synthesis of antenna arrays using artificial bee colony optimization algorithm," *Int. J. Microw. Opt. Technol.*, vol. 6, no. 4, pp. 234–241, 2011.

[9] A. Deb, J. S. Roy, and B. Gupta, "Performance comparison of differential evolution, particle swarm optimization and genetic algorithm in the design of circularly polarized microstrip antennas," *IEEE Trans. Antennas Propag.*, vol. 62, no. 8, pp. 3920–3928, Aug. 2014.

[10] M. Kovaleva, D. Bulger, and K. P. Esselle, "Comparative study of optimization algorithms on the design of broadband antennas," *IEEE J. Multiscale Multiphys. Comput. Techn.*, vol. 5, pp. 89–98, Jun. 2020. [Online]. Available: https://ieeexplore.ieee.org/document/9110788

[11] A. Chatterjee, G. K. Mahanti, and N. N. Pathak, "Comparative performance of gravitational search algorithm and modified particle swarm optimization algorithm for synthesis of thinned scanned concentric ring array antenna," *Progr. Electromagn. Res.*, vol. 25, pp. 331–348, Jan. 2010.

[12] S. Koziel and A. Pietrenko-Dabrowska, "Performance-based nested surrogate modeling of antenna input characteristics," *IEEE Trans. Antennas Propag.*, vol. 67, no. 5, pp. 2904–2912, May 2019.

[13] D. R. Prado, J. A. López-Fernández, M. Arrebola, and G. Goussetis, "Support vector regression to accelerate design and crosspolar optimization of shaped-beam Reflectarray antennas for space applications," *IEEE Trans. Antennas Propag.*, vol. 67, no. 3, pp. 1659–1668, Mar. 2019.

[14] M. R. Khan, C. L. Zekios, S. Bhardwaj, and S. V. Georgakopoulos, "Performance of random forest algorithm in high-dimensional surrogate modeling of antennas," in *Proc. IEEE Int. Symp. Antennas Propagat. USNC-URSI Radio Sci. Meeting (APS/URSI)*, 2021, pp. 1445–1446.

[15] S. Koziel and A. Pietrenko-Dabrowska, "Fast multi-objective optimization of antenna structures by means of data-driven surrogates and dimensionality reduction," *IEEE Access*, vol. 8, pp. 183300–183311, 2020.

[16] S. Koziel and A. Pietrenko-Dabrowska, "Design-oriented computationally-efficient feature-based surrogate modelling of multi-band antennas with nested kriging," *AEU-Int. J. Electron. Commun.*, vol. 120, Jun. 2020, Art. no. 153202.

[17] S. Koziel and A. Pietrenko-Dabrowska, "Rapid multi-objective optimization of antennas using nested kriging surrogates and single-fidelity EM simulation models," *Eng. Comput.*, vol. 27, no. 4, pp. 1491–1512, 2020.

[18] S. Koziel and A. Pietrenko-Dabrowska, "Recent advances in accelerated multi-objective design of high-frequency structures using knowledge-based constrained modeling approach," *Knowl.-Based Syst.*, vol. 214, Feb. 2021, Art. no. 106726.

[19] S. Koziel and A. T. Sigurdsson, "Triangulation-based constrained surrogate modeling of antennas," *IEEE Trans. Antennas Propag.*, vol. 66, no. 8, pp. 4170–4179, Aug. 2018.

[20] A. Massa, G. Oliveri, P. Rocca, and F. Viani, "System-by-design: A new paradigm for handling design complexity," in *Proc. 8th Eur. Conf. Antennas Propagat. (EuCAP)*, 2014, pp. 1180–1183.

[21] L. Wang, A. H. Ng, and K. Deb, *Multi-Objective Evolutionary Optimisation for Product Design and Manufacturing*. London, U.K.: Springer, 2011, doi: 10.1007/978-0-85729-652-8_1.

[22] E. Hancer, B. Xue, M. Zhang, D. Karaboga, and B. Akay, "Pareto front feature selection based on artificial bee colony optimization," *Inf. Sci.*, vol. 422, pp. 462–479, Jan. 2018.

[23] H. Li and Q. Zhang, "Multiobjective optimization problems with complicated Pareto sets, MOEA/D and NSGA-II," *IEEE Trans. Evol. Comput.*, vol. 13, no. 2, pp. 284–302, Apr. 2009.

[24] S. Chamaani, S. A. Mirtaheri, and M. S. Abrishamian, "Improvement of time and frequency domain performance of antipodal Vivaldi antenna using multi-objective particle swarm optimization," *IEEE Trans. Antennas Propag.*, vol. 59, no. 5, pp. 1738–1742, May 2011.

[25] Q.-Q. Li, Q.-X. Chu, Y.-L. Chang, and J. Dong, "Tri-objective compact log-periodic dipole array antenna design using MOEA/D-GPSO," *IEEE Trans. Antennas Propag.*, vol. 68, no. 4, pp. 2714–2723, Apr. 2020.

[26] A. J. Kerkhoff and H. Ling, "Design of a band-notched planar monopole antenna using genetic algorithm optimization," *IEEE Trans. Antennas Propag.*, vol. 55, no. 3, pp. 604–610, Mar. 2007.

[27] Y. Kuwahara, "Multiobjective optimization design of Yagi-Uda antenna," *IEEE Trans. Antennas Propag.*, vol. 53, no. 6, pp. 1984–1992, Jun. 2005.

[28] U. Singh, H. Kumar, and T. S. Kamal, "Design of Yagi-Uda antenna using biogeography based optimization," *IEEE Trans. Antennas Propag.*, vol. 58, no. 10, pp. 3375–3379, Oct. 010.

[29] A. Das, D. Mandal, S. Ghoshal, and R. Kar, "Concentric circular antenna array synthesis for side lobe suppression using moth flame optimization," *AEU-Int. J. Electron. Commun.*, vol. 86, pp. 177–184, Mar. 2018.

[30] U. Singh and M. Rattan, "Design of linear and circular antenna arrays using cuckoo optimization algorithm," *Progr. Electromagn. Res.*, vol. 46, pp. 1–11, Jan. 2014.

[31] E. A. Jones and W. T. Joines, "Design of Yagi-Uda antennas using genetic algorithms," *IEEE Trans. Antennas Propag.*, vol. 45, no. 9, pp. 1386–1392, Sep. 1997.

[32] S.-H. Yang and J.-F. Kiang, "Optimization of sparse linear arrays using harmony search algorithms," *IEEE Trans. Antennas Propag.*, vol. 63, no. 11, pp. 4732–4738, Nov. 2015.

[33] R. T. Marler and J. S. Arora, "Survey of multi-objective optimization methods for engineering," *Struct. Multidiscipl. Optim.*, vol. 26, no. 6, pp. 369–395, 2004.

[34] Y.-B. Tian and J. Qian, "Improve the performance of a linear array by changing the spaces among array elements in terms of genetic algorithm," *IEEE Trans. Antennas Propag.*, vol. 53, no. 7, pp. 2226–2230, Jul. 2005.

[35] P. Baumgartner *et al.*, "Multi-objective optimization of Yagi–Uda antenna applying enhanced firefly algorithm with adaptive cost function," *IEEE Trans. Magn.*, vol. 54, no. 3, pp. 1–4, Mar. 2018.

[36] M. R. Khan, C. L. Zekios, S. Bhardwaj, and S. V. Georgakopoulos, "Multi-objective optimization of an origami Yagi-Uda antenna using an adaptive fitness function," in *Proc. IEEE Int. Symp. Antennas Propag. North Amer. Radio Sci. Meeting*, 2020, pp. 2039–2040.

[37] N. N. Pathak, G. K. Mahanti, S. K. Singh, J. K. Mishra, and A. Chakraborty, "Synthesis of thinned planar circular array antennas using modified particle swarm optimization," *Progr. Electromagn. Res.*, vol. 12, pp. 87–97, Jan. 2009.
[38] J. D. Lohn, W. F. Kraus, D. S. Linden, and S. P. Colombano, "Evolutionary optimization of Yagi-Uda antennas," in *Proc. Int. Conf. Evol. Syst.*, 2001, pp. 236–243.
[39] A. A. Minai and R. D. Williams, "On the derivatives of the sigmoid," *Neural Netw.*, vol. 6, no. 6, pp. 845–853, 1993.
[40] Y. LeCun, Y. Bengio, and G. Hinton, "Deep learning," *Nature*, vol. 521, no. 7553, pp. 436–444, 2015.
[41] S. Haykin, *Neural Networks: A Comprehensive Foundation*. Upper Saddle River, NJ, USA: Prentice Hall PTR, 1994.
[42] R. Eberhart and J. Kennedy, "Particle swarm optimization," in *Proc. IEEE Int. Conf. Neural Netw.*, vol. 4, 1995, pp. 1942–1948.
[43] J. Robinson and Y. Rahmat-Samii, "Particle swarm optimization in electromagnetics," *IEEE Trans. Antennas Propag.*, vol. 52, no. 2, pp. 397–407, Feb. 2004.
[44] C. P. Birch, "A new generalized logistic sigmoid growth equation compared with the Richards growth equation," *Ann. Botany*, vol. 83, no. 6, pp. 713–723, 1999.
[45] D. P. Bertsekas, "Nondifferentiable optimization via approximation," in *Nondifferentiable Optimization*. Heidelberg, Germany: Springer, 1975, pp. 1–25.
[46] N. Jin and Y. Rahmat-Samii, "Advances in particle swarm optimization for antenna designs: Real-number, binary, single-objective and multiobjective implementations," *IEEE Trans. Antennas Propag.*, vol. 55, no. 3, pp. 556–567, Mar. 2007.
[47] S. Bhardwaj, N. K. Nahar, and J. L. Volakis, "Radial line slot array antenna with vertical waveguide feed for F-band communication," *IET Microw. Antennas Propag.*, vol. 9, no. 3, pp. 193–199, 2014.
[48] M. Clerc and J. Kennedy, "The particle swarm—Explosion, stability, and convergence in a multidimensional complex space," *IEEE Trans. Evol. Comput.*, vol. 6, no. 1, pp. 58–73, Feb. 2002.
[49] C. A. C. Coello, G. T. Pulido, and M. S. Lechuga, "Handling multiple objectives with particle swarm optimization," *IEEE Trans. Evol. Comput.*, vol. 8, no. 3, pp. 256–279, Jun. 2004.
[50] C. A. Balanis, *Antenna Theory: Analysis and Design*. New York, NY, USA: Wiley, 2016.
[51] L. Polo-López, J. Córcoles, and J. A. Ruiz-Cruz, "Antenna design by means of the fruit fly optimization algorithm," *Electronics*, vol. 7, no. 1, p. 3, 2018.
[52] M. Mohammadi-Parastoo, S. Mohammad-Ali-Nezhad, and S. Saviz, "Field-matching at the compact SIW horn antenna aperture using genetic algorithm," *Int. J. Numer. Model. Electron. Netw. Devices Fields*, vol. 33, no. 5, 2020, Art. no. e2738.
[53] K. Miura and R. Lang, "The science of Miura-ori: A review," in *Origami*, vol. 4. Natick, MA, USA: CRC Press, 2009, pp. 87–99.
[54] M. R. Khan, C. L. Zekios, S. V. Georgakopoulos, and S. Bhardwaj, "Automated CAD and modeling of origami structures for reconfigurable antenna applications," in *Proc. Int. Appl. Comput. Electromagn. Soc. Symp. (ACES)*, 2019, pp. 1–2.
[55] M. R. Khan, C. L. Zekios, S. Georgakopoulos, and S. Bhardwaj, "Automated design and optimization of origami electromagnetic structures [EM programmer's notebook]," *IEEE Antennas Propag. Mag.*, vol. 63, no. 2, pp. 89–102, Apr. 2021.
[56] S.-H. Wi, Y.-S. Lee, and J.-G. Yook, "Wideband microstrip patch antenna with U-shaped parasitic elements," *IEEE Trans. Antennas Propag.*, vol. 55, no. 4, pp. 1196–1199, Apr. 2007.

**MD RAYHAN KHAN** (Graduate Student Member, IEEE) was born in Dhaka, Bangladesh. He received the B.Sc. degree in electrical and electronic engineering from the Bangladesh University of Engineering & Technology, Dhaka, in 2016. He is currently pursuing the Ph.D. degree in electrical and computer engineering with the Florida International University (FIU), Miami, FL, USA.

He is working as a Graduate Research Assistant with the Department of Electrical and Computer Engineering, FIU. His research interests include optimization techniques, antennas, antenna arrays, computational electromagnetics, and machine learning.

**CONSTANTINOS L. ZEKIOS** (Senior Member, IEEE) received the Diploma degree (with Hons.) in electrical and computer engineering, the M.S. degree (with Hons.) in electrical and computer engineering communication and satellite telecommunication systems, and the Ph.D. degree (with Hons.) in electrical and computer engineering from the Democritus University of Thrace, Xanthi, Greece, in 2008, 2011, and 2015, respectively. From January 2016 to May 2018, he was a Postdoctoral Researcher with the Electrical and Computer Engineering Department, University of Massachusetts Amherst, Amherst, MA, USA, and from May 2018 to August 2020 he was a Fellow Postdoctoral Researcher with the Transforming Antennas Center, Florida International University, Miami, FL, USA, where he is currently a Research Assistant Professor with the Department of Electrical and Computer Engineering. His main research interests include computational electromagnetics, optimization methods, photonics, antennas, antenna arrays, electromagnetic surfaces, beamforming networks, and microwave engineering.

**SHUBHENDU BHARDWAJ** (Member, IEEE) received the B.Tech. degree *(summa cum laude)* in electronics engineering from IIT-Dhanbad, India, in 2004, the M.S. degree from UCLA, Los Angeles, CA, USA, in 2012, and the Ph.D. degree from The Ohio State University, Columbus, OH, USA, in 2017.

Since 2017, he has been an Assistant Professor with the Electrical and Computer Engineering Department, Florida International University, Miami, FL, USA. He is currently working on different topics within electromagnetics, including computational electromagnetics, power harvesting, terahertz devices, slow-wave structures, and sub-mm-wave/terahertz antennas. He is a recipient of the best student paper awards at URSI- GASS-2017, IEEE-iWat-2017, and IEEE-AMTA-2015. His paper also received the Second Place at Student Paper Competition at AMTA-2014 and honorable mentions at APS-2014 and 2015.

**STAVROS V. GEORGAKOPOULOS** (Senior Member, IEEE) received the Diploma degree in electrical engineering from the University of Patras, Patras, Greece, in June 1996, and the M.S. and Ph.D. degrees in electrical engineering from Arizona State University, Tempe, AZ, USA, in 1998 and 2001, respectively.

From 2001 to 2007, he held a position as the Principal Engineer with SV Microwave, Inc. Since 2007, he has been with the Department of Electrical and Computer Engineering, Florida International University, Miami, FL, USA, where he is currently a Professor, the Director of the Transforming Antennas Center (a research center on foldable/origami, physically reconfigurable, and deployable antennas), and the Director of the RF Communications, Millimeter-Waves, and Terahertz Lab. His current research interests relate to novel antennas, arrays, RFID, microwave and RF systems, novel sensors, and wireless powering of portable, wearable, and implantable devices. He received the 2015 FIU President's Council Worlds Ahead Faculty Award, which is the highest honor FIU extends to a faculty member for excelling in research, teaching, mentorship, and service. He served as an Associate Editor of the IEEE TRANSACTIONS ON ANTENNAS AND PROPAGATION from 2013 to 2019, and he has been currently serves as an Associate Editor of the IEEE OPEN JOURNAL OF ANTENNAS AND PROPAGATION since 2019.